Nanoscale

COMMUNICATION

Patterned porous silicon photonic crystals with modular surface chemistry for spatial control of neural stem cell differentiation†

Tiffany H. Huang,‡[a] Yi Pei,‡[a] Douglas Zhang,[a] Yanfen Li[b] and Kristopher A. Kilian*[a,b]

Cite this: *Nanoscale*, 2016, **8**, 10891

Received 24th November 2015,
Accepted 9th May 2016

DOI: 10.1039/c5nr08327c

www.rsc.org/nanoscale

We present a strategy to spatially define regions of gold and nanostructured silicon photonics, each with materials-specific surface chemistry, for azide–alkyne cycloaddition of different bioactive peptides. Neural stem cells are spatially directed to undergo neurogenesis and astrogenesis as a function of both surface properties and peptide identity.

An emerging area of broad technological importance is the integration of live cells with electronic, plasmonic and photonic materials.[1,2] In particular, cells of the central nervous system show great promise for a range of applications including: neuroprosthetics, neural circuits on a chip, and live cell biosensing.[3,4] Neural stem cells (NSCs) are a strong candidate cell type for these applications because they have the propensity to differentiate to multiple lineages of the central nervous system including neurons, astrocytes and oligodendrocytes.[5] NSCs have been shown to specify lineage in response to a myriad of materials-based cues including substrate stiffness,[6–8] nanotopography,[9,10] and matrix identity.[11] Short peptides derived from extracellular matrix proteins have been demonstrated to exert an influence on differentiation when grafted to a materials surface.[12–16] For instance, Stupp and colleagues showed how the presentation of the IKVAV peptide from laminin on peptide amphiphiles would direct NSCs to undergo neurogenesis[12] and Letourneau and co-workers showed how neurons will align with a gradient of IKVAV peptide.[17] Similarly other short peptides derived from the extracellular matrix have been demonstrated to elicit specific differentiation outcomes.[18]

An exciting optical material for integration with cells of the central nervous system is nanostructured porous silicon (PSi) because of its tunable optics and biocompatibility,[19] ease of fabrication and integration with silicon processing technology,[20] and potential for lithographic patterning towards spatially defined optoelectronic devices.[21,22] PSi is formed by electrochemical etching of single crystal silicon in hydrofluoric acid electrolyte. By changing the applied current density during etching, the porosity can be varied to incorporate a well-defined refractive index profile that can be tuned to establish a photonic bandgap. These PSi-based photonic crystals have attracted interest as biosensors,[23–26] drug delivery vehicles,[27,28] and "smart" cell culture substrates.[29,30] PSi has been demonstrated as a viable optical substrate for the culture of neuronal cells,[31,32] including integration with dissimilar nanomaterials.[33]

When fabricating complex devices that require interconnects and arrays of features, patterning approaches based on lithography can enable mixing of diverse classes of materials. Porous silicon has been patterned using a number of lithography based strategies. Previous reports have used either n-type silicon with photomasks to define the etch regions[34] or through patterning the silicon wafer first using various masking techniques.[35,36] Alternative approaches using chemistry have been employed recently to pattern PSi. For instance, Gooding and colleagues recently developed a multistep approach to pattern chemically modified PSi using photolithography and demonstrated the applicability for cell microarrays with an optical read-out.[37] Similarly, Voelcker and colleagues showed how photochemical hydrosilylation could be used to specifically modify select regions with one chemistry followed by introducing a second chemistry on the remaining surface.[38] In the study presented here we show how lithographically patterned gold–PSi substrates, that are functionalized with bioactive peptides derived from extracellular matrix proteins, can be used to guide neurogenesis and astrogenesis programs in adherent NSCs.

We used photolithography to expose different patterns across a silicon substrate followed by e-beam evaporation of a thin adhesion layer of titanium (5 nm) and gold (100 nm) (Fig. 1). Next, the resist was removed and the gold patterned silicon placed in an electrochemical etching cell. We chose to

[a]*Department of Materials Science and Engineering, University of Illinois at Urbana-Champaign, Urbana, IL 61874, USA. E-mail: kakilian@illinois.edu*

[b]*Department of Bioengineering, University of Illinois at Urbana-Champaign, Urbana, IL 61874, USA*

†Electronic supplementary information (ESI) available. See DOI: 10.1039/c5nr08327c

‡These authors contributed equally to this work.

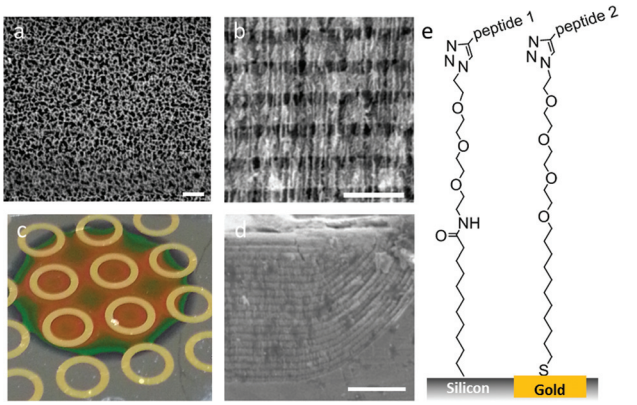

Fig. 1 (a) Top view scanning electron micrograph of porous silicon. Scale bar 100 nm. (b) Side view scanning electron micrograph of Bragg mirror structure demonstrating alternating regions of low and high porosity. Scale bar 100 nm. (c) Photograph of patterned gold rings on nanostructured porous silicon. (d) Side view scanning electron micrograph of porous silicon under-etched at the perimeter of a gold island. Scale bar 1 μm. (e) Schematic of functionalization chemistry for silicon and gold regions.

fabricate PSi distributed Bragg reflectors in the regions between the gold because these optical materials have previously been demonstrated to serve as good sensing motifs, and the nanoarchitecture can be appropriately tuned to influence cell adhesion.[39,40] Using an alternating step function of high and low porosity yields a nanostructured material where the high porosity top layer shows pore diameters on the order of ~10–50 nm (Fig. 1a). Scanning electron microscopy of the profile shows how modulating the current density can lead to regions with different porosity in the multilayered stack (Fig. 1b). While the gold remains uniform during the etch, there is a small undercut beneath the gold perimeter that leads to an arc-like morphology. Nevertheless, optical characterization of the Bragg mirror demonstrates a high reflectivity between 900 and 1000 nm in-line with the etching parameters (Fig. 2a).

Freshly etched porous silicon will oxidize in aqueous environments, and requires chemical passivation to stabilize the surface.[41] Hydrosilylation of alkenes and alkynes has been demonstrated to form a very stable Si–C bond at the surface, thus protecting the underlying silicon from the ingress of water.[42] The gold–PSi was immersed in a degassed solution of

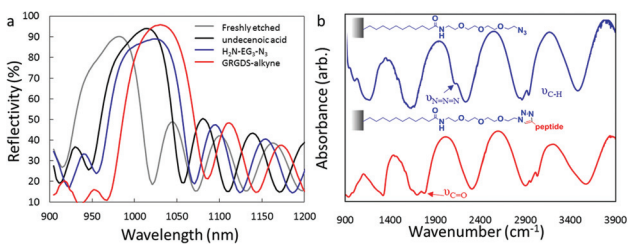

Fig. 2 (a) Reflectivity spectra of a porous silicon Bragg mirror during chemical modification. (b) Fourier transform infrared characterization of chemical modification.

the neat alkene undecenoic acid under argon atmosphere, and reacted at 100 °C for 4 hours. After hydrosilylation the Bragg plateau shifts 31 nm, which indicates the bulk refractive index has changed after replacing air with organic material at the pore walls (Fig. 2a). The carboxylic acid headgroup was further reacted with 1-ethyl-3-(3-dimethylaminopropyl)carbodiimide (EDC) and *N*-hydroxysuccinimide (NHS) followed by conjugation of an amino oligo(ethylene glycol) azide (H_2N–EG_3–N_3) to form the amide containing a distal azide moiety. The ethylene glycol groups serve the purpose of preventing non-specific protein adsorption to the interface that would prevent specific interactions with immobilized peptides. Addition of the H_2N–EG_3–N_3 leads to a further red shift in the Bragg plateau of 10 nm. Next, alkyne terminated peptides were conjugated using an azide–alkyne cycloaddition "click" reaction. We chose to study three bioactive peptides known to support cell adhesion: (1) IKVAV derived from the α1 chain of laminin, (2) YIGSR derived from the β1 chain of laminin, and (3) GRGDS derived from fibronectin. After coupling of peptide, we see a further red shift in the reflectivity spectrum (Fig. 2a; 25 nm shift with GRGDS).

Forming organic multilayers within the nanoarchitecture of PSi photonic crystals can be easily monitored *via* the silicon photonics, where the sign and magnitude of the shift is indicative of a well-formed layer. To support the results of changes in optical properties during our chemical modification, we also performed Fourier transform infrared spectroscopy (FTIR) on the porous film. Fig. 2b shows the FTIR absorbance spectra for the azide terminated surface and after cycloaddition of the alkyne-peptide. While a large interference fringe from reflection at the top and base of the film dominates the spectra, modes associated with chemical functionalities can be readily discerned. The azide terminated surface shows a strong azide stretching band at 2127 cm^{-1} and C–H stretching modes at ~2800–3000 cm^{-1}. After azide–alkyne cycloaddition, the azide stretching peak disappears indicating successful "click" reaction, and we see carbonyl stretching for the carboxylic acid of the peptide (1784 cm^{-1}) and the amide backbone (1687 cm^{-1}).[43,44]

After successful monolayer formation on the PSi, we immersed the sample in a solution of HS–C11–EG_3 containing 15% of the azide terminated alkanethiolate HS–C11–EG_4–N_3 to form a mixed monolayer. We chose to dilute the azide moiety because our previous work has demonstrated an optimal surface density of peptides for promoting adhesion and differentiation using mesenchymal stem cells[15] and adipose derived stem cells.[45] Too high a density will disallow efficient biorecognition *via* cell surface receptors. Alkyne terminated peptides were then immobilized *via* azide–alkyne cycloaddition. To verify successful immobilization of peptide to the gold substrates, we used the scrambled adhesion sequence GRGDS as a negative cell adhesion control (Fig. 3a).

Previous work has demonstrated that the ingress of biomolecules into the nanoporous architecture will lead to a red shift in the optics of the photonic crystal due to replacing water with organic material.[29] To explore whether secretion by

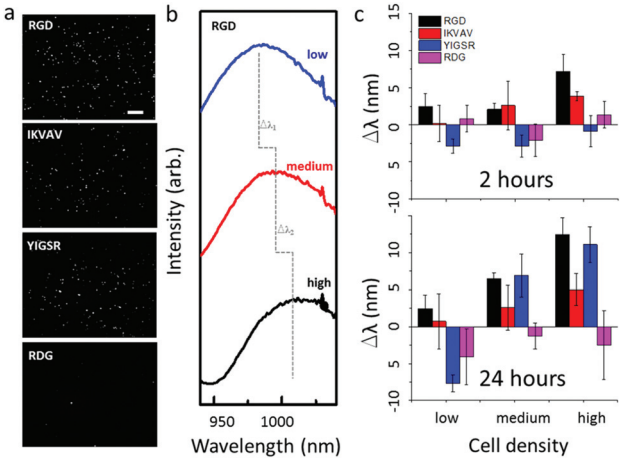

Fig. 3 (a) Binary nuclei images of NSCs adherent to peptide modified PSi (scale bar 200 μm). (b) Reflectivity spectra of a Bragg mirror shifting in response to a low, medium and high cell density. (c) Quantification of the reflectivity shift for peptide modified surfaces with different cell seeding densities after 2 hours and 24 hours.

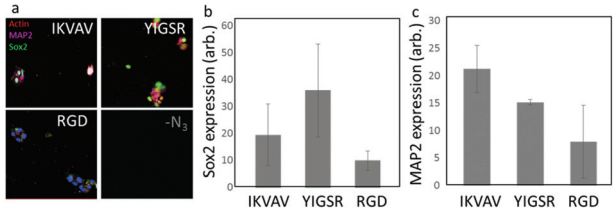

Fig. 4 (a) Immunofluorescence images of neural stem cells adherent to peptide modified porous silicon with azide control. (b) Quantitation of Sox2 and (c) MAP2 expression from adherent neural stem cells.

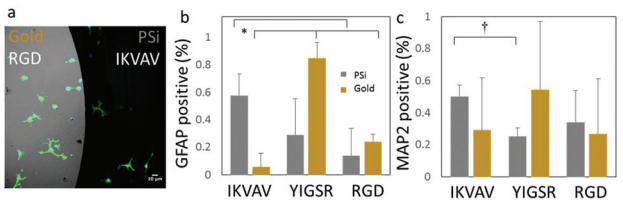

Fig. 5 (a) Phase contrast/fluorescence overlay of NSCs adherent to patterned PSi–gold substrates (green-actin; blue; nuclei). Quantitation of astrocyte (b, GFAP) and neuron (c, MAP2) expression for cells cultured on peptide modified porous silicon and gold surfaces. *p-Value 0.03; †p-value 0.0003.

adherent cells could be monitored by assessing the optics of the underlying photonic crystal, we seeded rat neural stem cells (NSCs) on the patterned substrate where each material contained a specific bioactive peptide. Fig. S1† shows that NSCs adhere uniformly across the patterned materials. After 2 and 24 hours the optical properties of the Bragg mirrors were assessed. Fig. 3b shows a representative spectra of the Bragg mirror after culture with NSCs at low (1.1×10^5), medium (2.0×10^5) and high (6.4×10^5) cell seeding density. In each case there is a red-shift associated with increased cell number. Interestingly, while cell number is comparable across the different adhesion peptides, the magnitude of the shift varies with surface peptide identity and incubation time (Fig. 3c). Importantly, there are few adherent cells on the RDG peptide and the reflectivity shift does not correlate with cell seeding density. Indeed the RDG functionalized PSi undergoes a blue shift indicating oxidation of the underlying PSi. These result suggests that optical materials may be used to monitor cellular secretion *in situ*, which could prove useful in studying biological processes in adherent cells.

To ascertain the expression of markers associated with neural fates, we immunostained the adherent cells with the NSC multipotency marker Sox2 and the neuronal marker microtubule associated protein 2 (MAP2). NSCs adherent to IKVAV show elevated expression of the neuronal marker MAP2 while those adherent to YIGSR show the highest expression of the stem cell marker Sox2 (Fig. 4). Cells adherent to RGD show low expression of both markers. This result is consistent with previous studies demonstrating enhanced neurogenesis when NSCs are exposed to the peptide IKVAV.[12] To explore whether NSCs adherent to our surfaces are undergoing astrogenesis, we immunostained for the astrocyte marker glial fibrillary acidic protein (GFAP). In general, the peptide IKVAV promotes expression of both MAP2 and GFAP compared to YIGSR and RGD. However, when we vary bioactive peptide on the PSi surface while keeping the gold patterns modified with RGD we see an interesting trend in expression between populations (Fig. 5). NSCs adherent to PSi modified with IKVAV express elevated levels of GFAP and MAP2, while cells on adjacent RGD modified gold show reduced expression. In contrast, NSCs adherent to YIGSR show modest expression of GFAP and MAP2, while at the same time cells on adjacent RGD modified gold show a large enhancement in both GFAP and MAP2 expression. When both materials are modified with RGD we see relatively low expression of both markers. Taken together, this result suggests that adhesive and soluble signals coordinate lineage specification in discreet populations of cells to regulate different outcomes spatially across the substrate. More work is necessary to deconstruct the interplay between cell–cell, cell–matrix and soluble signalling during differentiation on peptide patterned materials.

Conclusions

In summary, we show how a combination of lithographic patterning and control of surface chemistry can be used to spatially direct NSC differentiation across patterned gold and silicon-based photonic crystals. Bioactive peptides from laminin are shown to coordinate neurogenesis and astrogenesis in the absence of soluble differentiation promoting cues. The use of nanostructured porous silicon will enable remote interrogation of the optical properties of the underlying substrate to monitor signalling from adherent cells. Similarly, the use of gold may allow for plasmonic or electronic

sensing strategies to complement the photonics, in a spatially addressable fashion. Furthermore, the high surface area mesoporous network in PSi can be loaded with drug which may prove useful in guiding the differentiation of adherent cells. The controlled differentiation of NSCs through surface chemistry alone on multifunctional assemblies of optical and electronic materials will prove useful in fundamental studies of cell adhesion and differentiation, and will also aid the design of next generation devices that integrate electronic materials with cells of the central nervous system.

Acknowledgements

This work was supported by the National Science Foundation grant number 1454616. We thank Neil Krueger and Prof. Paul Braun for helpful discussions and assistance with etching optimization.

Notes and references

1 A. Simi, H. Amin, A. Maccione, T. Nieus and L. Berdondini, *Prog. Brain Res.*, 2014, **214**, 415–442.
2 N. A. Kotov, J. O. Winter, I. P. Clements, E. Jan, B. P. Timko, S. Campidelli, S. Pathak, A. Mazzatenta, C. M. Lieber, M. Prato, R. V. Bellamkonda, G. A. Silva, N. W. S. Kam, F. Patolsky and L. Ballerini, *Adv. Mater.*, 2009, **21**, 3970–4004.
3 D. Borton, S. Micera, J. D. R. Millan and G. Courtine, *Sci. Transl. Med.*, 2013, **5**, 210rv212.
4 A. K. Soe, S. Nahavandi and K. Khoshmanesh, *Biosens. Bioelectron.*, 2012, **35**, 1–13.
5 O. Gonzalez-Perez, *Biol. Biomed. Rep.*, 2012, **2**, 59–69.
6 S. Musah, P. J. Wrighton, Y. Zaltsman, X. Zhong, S. Zorn, M. B. Parlato, C. Hsiao, S. P. Palecek, Q. Chang, W. L. Murphy and L. L. Kiessling, *Proc. Natl. Acad. Sci. U. S. A.*, 2014, **111**, 13805–13810.
7 N. D. Leipzig and M. S. Shoichet, *Biomaterials*, 2009, **30**, 6867–6878.
8 J. Arulmoli, M. M. Pathak, L. P. McDonnell, J. L. Nourse, F. Tombola, J. C. Earthman and L. A. Flanagan, *Sci. Rep.*, 2015, **5**, 8499.
9 K. Yang, K. Jung, E. Ko, J. Kim, K. I. Park, J. Kim and S.-W. Cho, *ACS Appl. Mater. Interfaces*, 2013, **5**, 10529–10540.
10 S. Ankam, C. K. Lim and E. K. F. Yim, *Biomaterials*, 2015, **47**, 20–28.
11 I. Kazanis and C. Ffrench-Constant, *Dev. Neurobiol.*, 2011, **71**, 1006–1017.
12 G. A. Silva, C. Czeisler, K. L. Niece, E. Beniash, D. A. Harrington, J. A. Kessler and S. I. Stupp, *Science*, 2004, **303**, 1352–1355.
13 T.-Y. Cheng, M.-H. Chen, W.-H. Chang, M.-Y. Huang and T.-W. Wang, *Biomaterials*, 2013, **34**, 2005–2016.
14 E. J. Berns, S. Sur, L. Pan, J. E. Goldberger, S. Suresh, S. Zhang, J. A. Kessler and S. I. Stupp, *Biomaterials*, 2014, **35**, 185–195.
15 K. A. Kilian and M. Mrksich, *Angew. Chem., Int. Ed.*, 2012, **51**, 4891–4895.
16 B. Ananthanarayanan, L. Little, D. V. Schaffer, K. E. Healy and M. Tirrell, *Biomaterials*, 2010, **31**, 8706–8715.
17 D. N. Adams, E. Y. C. Kao, C. L. Hypolite, M. D. Distefano, W.-S. Hu and P. C. Letourneau, *J. Neurobiol.*, 2004, **62**, 134–147.
18 G.-H. Cui, S.-J. Shao, J.-J. Yang, J.-R. Liu and H.-D. Guo, *Mol. Neurobiol.*, 2016, **53**, 1108–1123.
19 M. P. Stewart and J. M. Buriak, *Adv. Mater.*, 2000, **12**, 859–869.
20 A. G. Cullis, L. T. Canham and P. D. J. Calcott, *Appl. Phys. Rev.*, 1997, **82**, 909–956.
21 Y. Y. Li, V. S. Kollengode and M. J. Sailor, *Adv. Mater.*, 2005, **17**, 1249–1251.
22 H. Wang, B. Welker, Y. Gao, J. F. Federici and R. A. Levy, *Mater. Lett.*, 1995, **23**, 209–214.
23 M. P. Stewart and J. M. Buriak, *Adv. Mater.*, 2000, **12**, 859–869.
24 S. D'Auria, M. de Champdore, V. Aurilia, A. Parracino, M. Staiano, A. Vitale, M. Rossi, I. Rea, L. Rotiroti, A. M. Rossi, S. Borini, I. Rendina and L. De Stefano, *J. Phys.: Condens. Matter*, 2006, **18**, S2019–S2028.
25 G. Marsh, *Mater. Today*, 2002, **5**, 36–41.
26 T. Islam and H. Saha, *Sens. Actuators, A*, 2007, **133**, 472–479.
27 K. L. Jarvis, T. J. Barnes and C. A. Prestidge, *Adv. Colloid Interface Sci.*, 2012, **175**, 25–38.
28 E. J. Anglin, L. Cheng, W. R. Freeman and M. J. Sailor, *Adv. Drug Delivery Rev.*, 2008, **60**, 1266–1277.
29 K. A. Kilian, L. M. H. Lai, A. Magenau, S. Cartland, T. Bocking, G. N. Di, M. Gal, K. Gaus and J. J. Gooding, *Nano Lett.*, 2009, **9**, 2021–2025.
30 M. P. Schwartz, A. M. Derfus, S. D. Alvarez, S. N. Bhatia and M. J. Sailor, *Langmuir*, 2006, **22**, 7084–7090.
31 G. Marinaro, R. La Rocca, A. Toma, M. Barberio, L. Cancedda, E. Di Fabrizio, P. Decuzzi and F. Gentile, *Integr. Biol.*, 2015, **7**, 184–197.
32 M. J. Sweetman, C. J. Shearer, J. G. Shapter and N. H. Voelcker, *Langmuir*, 2011, **27**, 9497–9503.
33 C. J. Shearer, F. J. Harding, M. J. Sweetman, J. G. Shapter and N. H. Voelcker, *Surf. Coat. Technol.*, 2013, **224**, 49–56.
34 S. Tuomikoski, K. Huikko, K. Grigoras, P. Ostman, R. Kostiainen, M. Baumann, J. Abian, T. Kotiaho and S. Franssila, *Lab Chip*, 2002, **2**, 247–253.
35 N. Nagy, A. E. Pap, E. Horvath, J. Volk, I. Barsony, A. Deak and Z. Horvolgyi, *Appl. Phys. Lett.*, 2006, **89**, 063104/063101–063104/063103.
36 M. Zahedinejad, M. Kaje, A. Erfanian, F. Raissi, H. Mehrara and F. Rezvani, *Thin Solid Films*, 2012, **520**, 2080–2084.
37 Y. Zhu, A. H. Soeriyadi, S. G. Parker, P. J. Reece and J. J. Gooding, *J. Mater. Chem. B*, 2014, **2**, 3582–3588.
38 M. J. Sweetman, M. Ronci, S. R. Ghaemi, J. E. Craig and N. H. Voelcker, *Adv. Funct. Mater.*, 2012, **22**, 1158–1166.
39 S. P. Low, K. A. Williams, L. T. Canham and N. H. Voelcker, *Biomaterials*, 2006, **27**, 4538–4546.

40 Y. L. Khung, G. Barritt and N. H. Voelcker, *Exp. Cell Res.*, 2008, **314**, 789–800.
41 K. A. Kilian, T. Boecking and J. J. Gooding, *Chem. Commun.*, 2009, 630–640, DOI: 10.1039/b815449j.
42 K. A. Kilian, T. Böcking, K. Gaus, M. Gal and J. J. Gooding, *Biomaterials*, 2007, **28**, 3055–3062.
43 S. Ciampi, T. Boecking, K. A. Kilian, J. B. Harper and J. J. Gooding, *Langmuir*, 2008, **24**, 5888–5892.
44 K. A. Kilian, T. Böcking, K. Gaus and J. J. Gooding, *ACS Nano*, 2007, **1**, 355–361.
45 D. Zhang and K. A. Kilian, *J. Mater. Chem. B*, 2014, **2**, 4280–4288.